JOURNAL OF MATERIALS SCIENCE 25 (1990) 3467–3474

Fracture behaviour and its relation to critical current of silver-sheathed $Ba_2YCu_3O_{7-x}$ superconducting composite wires and tapes

SHOJIRO OCHIAI, KENJI HAYASHI, KOZO OSAMURA
Department of Metallurgy, Faculty of Engineering, Kyoto University, Sakyo-ku, Kyoto 606, Japan

Silver-sheathed $Ba_2YCu_3O_{7-x}$ superconducting composite wires and tapes were prepared by rolling, drawing, swaging and pressing methods. The fracture behaviour and its influence on critical current at 0 T at 77 K of the $Ba_2YCu_3O_{7-x}$ were investigated. The oxide was found to show multiple fracture under applied tensile stress, and the critical current density and tensile strength of the oxide in the rolled, swaged and pressed samples were higher than those in the drawn samples. When the working amount was high, the current density and the strength of the oxide were found to become high. Within the present conditions, there was a correlation between critical current density and cracking stress: the higher the cracking stress, the higher the critical current density became. The cracking stress of the present oxide was determined to be 50 MPa at most, being far lower than that of the Nb_3Sn compound (800 to 2000 MPa). The critical current density of the rolled, swaged and pressed samples was reduced rapidly when exerted stress on the oxide exceeded the cracking stress, while the reduction in the drawn samples occurred gradually. A strong dependence of the critical current, as a function of applied stress and cracking stress of the oxide, on the measured portion due to scatter in the size of defects contained in the oxide, was found.

1. Introduction

Since Wu *et al.* [1] discovered that the Ba–Y–Cu–O oxide superconductor has a higher critical temperature (T_c) than the boiling point of liquid nitrogen, i.e. 77 K, extensive studies have been carried out to fabricate composite wire or tape, with the main aim to achieve high critical current density. However, mechanical behaviour, which is also important for practical application, and its relation to critical current density, have not been studied in detail. The aim of the present work was to investigate fracture behaviour of the $Ba_2YCu_3O_{7-x}$ in silver-sheathed composite wires and tapes and its relation to critical current.

2. Experimental procedure

The process for preparing composite wires and tapes is summarized in Fig. 1. The $BaCO_3$, Y_2O_3 and CuO powders were weighed in the composition ratio Ba : Y : Cu = 2 : 1 : 3 and mixed together. The mixtures were calcined at 1173 K for 173 ksec and then ground. To achieve high homogeneity, calcining and grinding were repeated three times, then silver tubes were filled with the powders. The following six working methods were applied to fabricate wire and tape at room temperature. (i) Some composite samples were swaged into prescribed diameters (S samples). Some composite samples were rolled with grooved rollers and formed into regular squares. After this, (ii) further rolling with grooved rollers (RG samples), (iii) rolling without grooves (R), (iv) drawing (D), (v) pressing at 0.5 GPa after drawing (DP), and (iv) pressing after rolling with grooved rollers (RGP samples) were carried out. In this work, the final diameter of the wires and the final thickness of the tapes are shown by the figures in units of millimetres following the sample name: for instance, R0.8 means the rolled sample with final thickness of 0.8 mm, and RGP1.0 means the sample 1.0 mm thick prepared by pressing after rolling with grooved rollers. Following the above cold-workings, all samples were annealed in an oxygen atmosphere at 1193 K for 43.2 ksec and then cooled in a furnace in the same atmosphere at a rate of 0.021 K sec^{-1}.

The critical current was measured at 0 T at 77 K with a criterion of 1 $\mu V\,cm^{-1}$ at various stress levels. In this work, in order to know the influence of gauge length on the critical current, the resistance probes were attached in steps of 2.5 mm, as shown in Fig. 2 in which 1 to 5 indicate their points of attachment. The critical current of the samples 10 mm long was measured from the resistance between 1 and 5 probes, and that for 2.5 mm from the resistance between i and $i + 1$ (i = 1 to 4) probes. The critical current density was calculated by dividing the critical current by the cross-sectional area of the oxide measured for the respective sample.

The tensile test was carried out at room temperature and 77 K with an Instron type tensile machine at a

0022–2461/90 $03.00 + .12

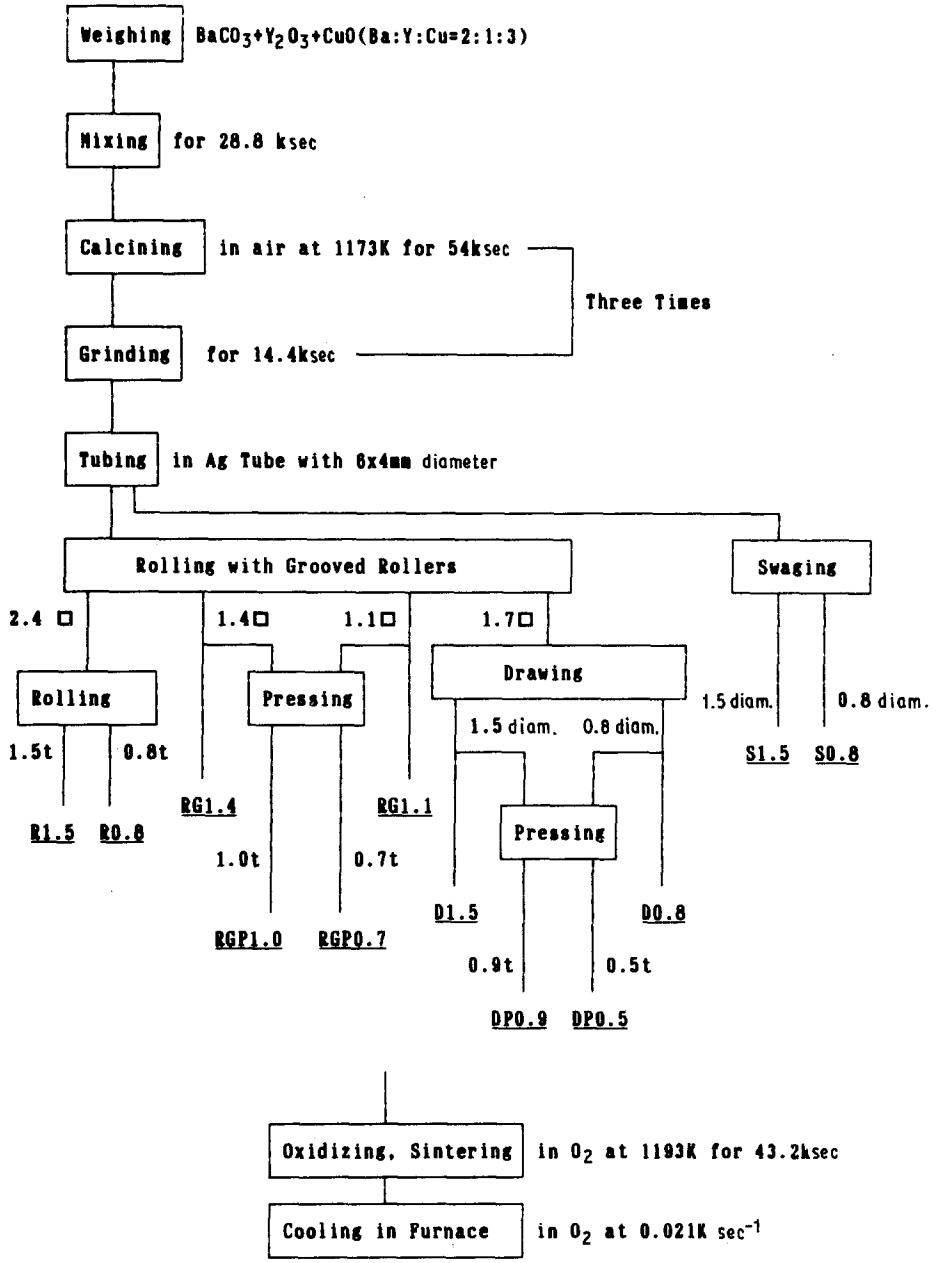

Figure 1 Process for preparing superconducting composite wires and tapes. t = thickness.

strain rate of 4.17×10^{-4} sec^{-1} for a gauge length of 20 mm. The appearance of the oxide core after stressing was observed with a scanning electron microscope, by etching away the silver sheath.

3. Experimental results and discussion

3.1. Stress–strain curve and fracture morphology

In the stress–strain curves of the R, RGP, DP and S samples, many drops in stress occurred but not in the curves of the D samples, as typically shown in Fig. 3 where the stress–strain curves of RGP0.7, S0.8 and D0.8 are representatively presented. Observation of the appearance of the oxide core in the former samples stressed to various levels revealed that the drop in stress was caused by cracking in the oxide. Typical morphologies of the oxide before and after stressing are shown below.

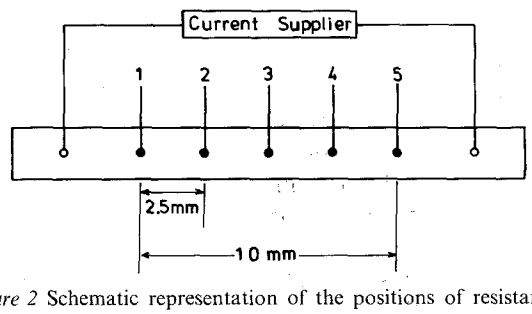

Figure 2 Schematic representation of the positions of resistance-probes for critical current measurements.

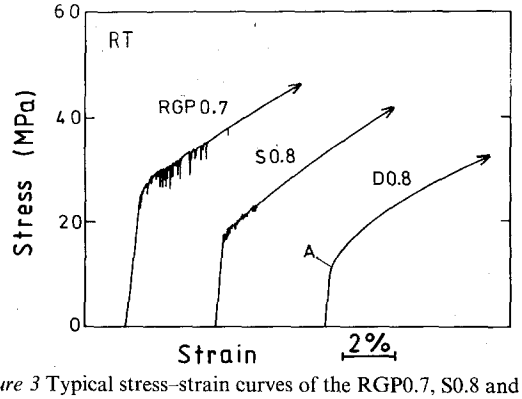

Figure 3 Typical stress–strain curves of the RGP0.7, S0.8 and D0.8 samples measured at room temperature.

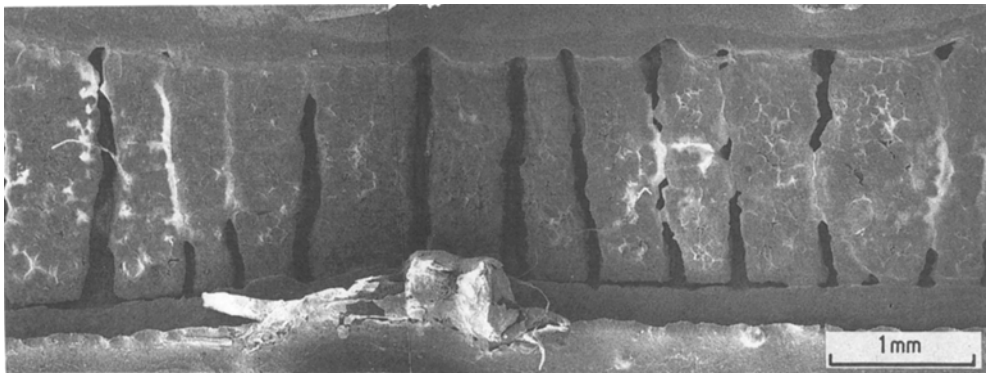

Figure 4 Typical appearance of the oxide in the R0.8 sample after stressing to cause fracture of the composite as a whole at room temperature.

Fig. 4 shows the fracture morphology of the oxide in the R0.8 sample after stressing to cause fracture of the composite tape as a whole. The oxide fractured nearly perpendicular to tensile axis. As a result of multiple cracking, the length of the segments became short. Fig. 5 shows the morphology of the RGP0.7 sample (a) before and (b, c) after stressing. In the RGP sample, longitudinal cracks existed even before stressing (a) while not in the R sample. The reason for this is unknown at present. In the RGP sample, the fracture of the oxide was sometimes stopped at longitudinal pre-existing cracks and sometimes not. The oxides in the S and DP samples showed similar behaviour to those in the R and RGP ones, respectively. The RG samples showed intermediate behaviour between R and RGP samples.

In the case of the D sample, cracks were observed in the oxide before stressing as shown in Fig. 6a. When the composite wires were stressed beyond the stress indicated by Ȧ in Fig. 3, at which the curve deviated from the linear relation between stress and strain, the pre-existing cracks propagated slowly and new observable cracks formed one after another, as shown in Figs 6b and c. In this sample, the growth of pre-existing cracks and also the formation of new cracks did not result in an observable drop in stress in the stress–strain curves, indicating that the oxide in these samples was very frail. The reason for this might be attributed to the tensile stress acting during drawing in these samples, introducing cracks, which could not be vanished by sintering.

The multiple fracture phenomenon has been observed in fibre-reinforced composite materials and also Nb_3Sn in bronze-processed composite wires [2–5]. This phenomenon occurs in a following manner [6, 7]. The breakdown of the oxide core in one cross-section causes a drop in load-bearing capacity of the composite. In this cross-section, however, the sheath work-

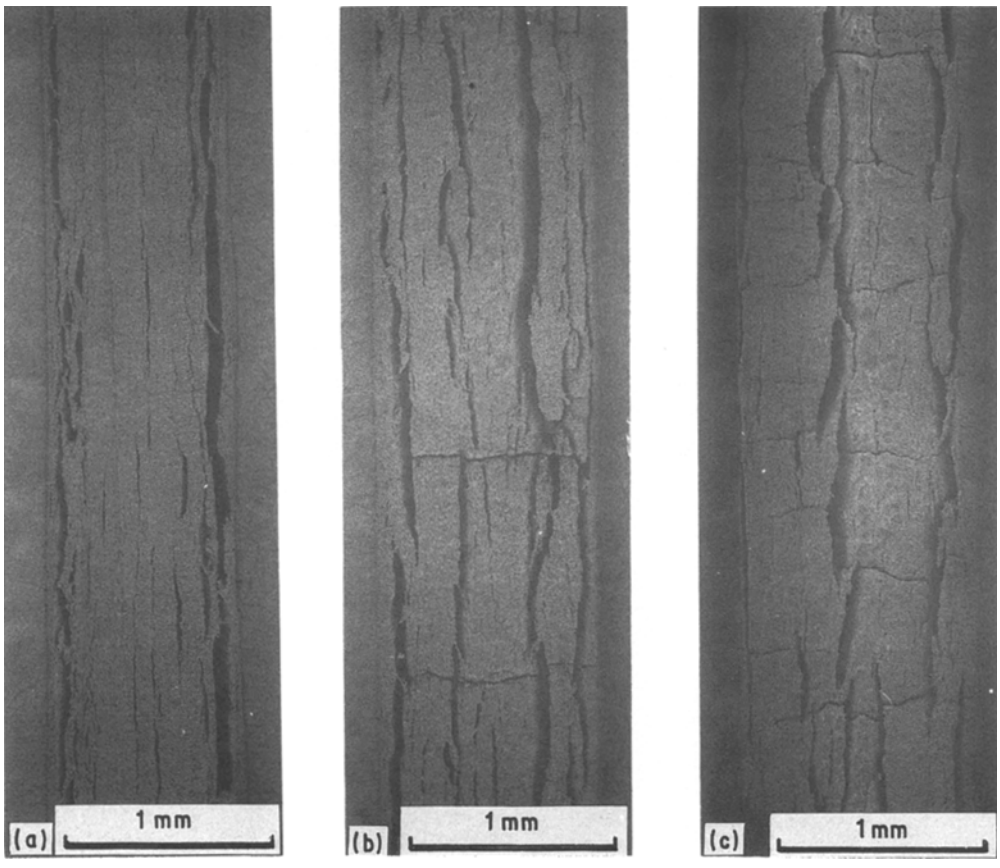

Figure 5 Typical appearance of the oxide in the RGP0.7 sample stressed at room temperature. (a) $\sigma_c = 0$, (b) $\sigma_c = 28$ MPa, (c) $\sigma_c = 34$ MPa.

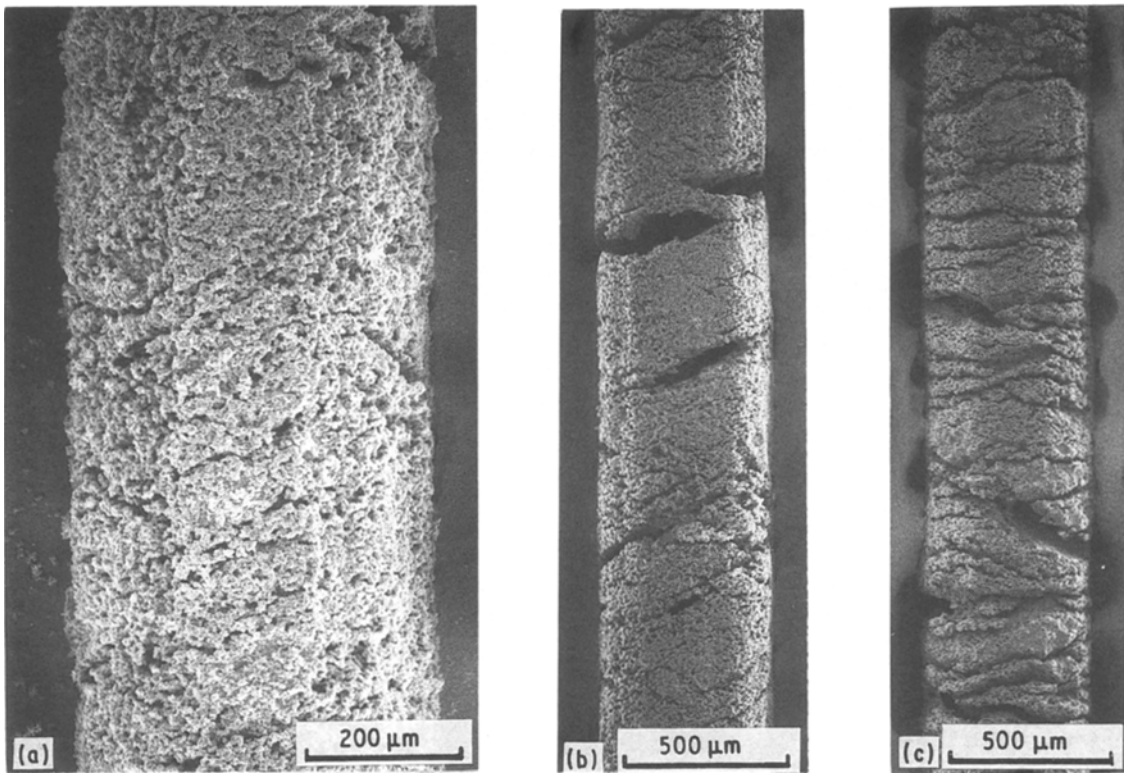

Figure 6 Typical appearance of the oxide in the D0.8 sample stressed at room temperature. (a) $\sigma_c = 0$, (b) $\sigma_c = 24$ MPa, (c) $\sigma_c = 45$ MPa.

hardens and then the load-bearing capacity of the cross-section rises again. During this process, stress is transferred to the oxide core by the shear stress at the core–sheath interface so that the core, once fractured, fails again in another cross-section. With a repetition of this process, the core fractures continually into shorter lengths.

3.2. Cracking stress of the oxide

The first drop in stress in the stress–strain curves is caused by the cracking of the weakest portion in the oxide in the case of S, R, RG, DP and RGP samples. The cracking stress of the oxide, σ_{1u}, for these samples was estimated from the stress of the composite at the first stress drop, σ_c', in the following way. For the D samples, σ_c' was, to a first approximation, taken from the stress at A in Fig. 3 at which stress deviates from the linear relation to strain, resulting in apparent plastic deformation of the composite as a whole, and σ_{1u} was inferred due to the following reason.

In the present D sample, the silver yielded in tension before stressing as shown later, due to the stress introduced by cooling from the annealing temperature to room temperature or 77 K, which arises from the difference in thermal expansion between the oxide and silver. Therefore, deviation from the linear relation at A in Fig. 3 cannot be attributed to the tensile yielding of silver. Another mechanism for the deviation is related to the multiple cracking. Once multiple cracking takes place, the stress of the composite as a whole deviates from the linear relation to strain as known from the stress–strain curves of the RGP0.7 and S0.8 samples shown in Fig. 3. Such a deviation has also been observed for the multiple cracking of the Nb_3Sn compound in the bronze-processed multifilamentary composite wire [3]. These experimental results indicate that cracking stress can be inferred from the composite stress at A in Fig. 3, to a first approximation. Of course, in this case, no apparent drop in stress was detected in the stress–strain curve, the stress at first cracking cannot be identified. In this work, the inferred values of σ_{1u} for the D samples will be used only for qualitative comparison with those for other samples.

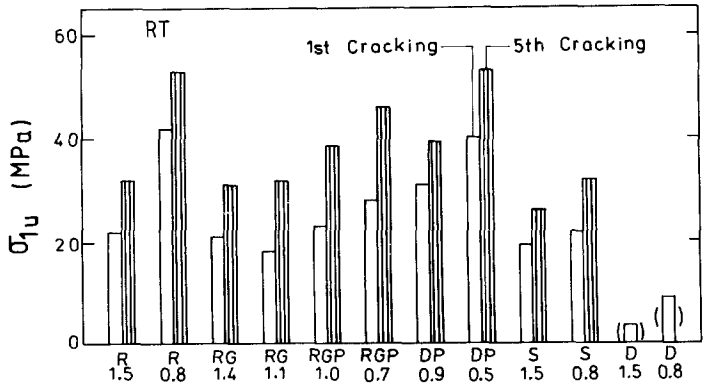

Figure 7 Cracking stresses to cause first and fifth crackings in the oxide at room temperature (average of three samples).

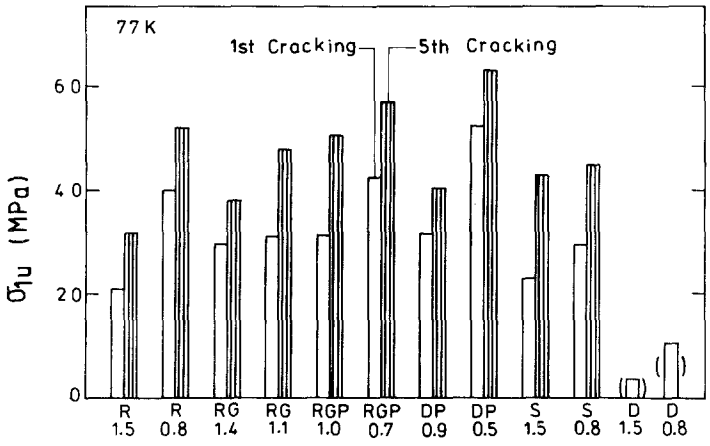

Figure 8 Cracking stresses to cause first and fifth crackings in the oxide at 77 K (average of three samples).

3.2.1. Estimation method of tensile strength of the oxide

As the coefficient of thermal expansion of the oxide is different from that of silver, residual stresses are exerted on them. The residual stresses were inferred as follows. The oxide core, the silver sheath and the composite as a whole are denoted 1, 2 and c, respectively.

The stress–strain (σ_2–e) curve of the sheath was expressed as follows, by approximating that the sheath shows linear strain hardening after yielding. In the stage of elastic deformation ($e < e_y$ where e_y is the yield strain in tension), σ_2 was given by

$$\sigma_2 = eE_2 \quad (1)$$

where E_2 is the Young's modulus of the sheath, and in the stage of plastic deformation ($e > e_y$), σ_2 was given by

$$\sigma_2 = (1 - \omega)\sigma_y + \omega eE_2 \quad (2)$$

where σ_y is the yield stress given by $e_y E_2$ and ω is the slope of the stress–strain curve in the stage of plastic deformation, normalized with respect to E_2. When the samples are cooled down from annealing temperature, T_A, to test temperature, T (room temperature and 77 K in this work), the residual strains of the core (e_{r1}) and sheath (e_{r2}) at room temperature are given by

$$e_{r1} = (\alpha_c - \alpha_1)(T - T_A) \quad (3)$$

$$e_{r2} = (\alpha_c - \alpha_2)(T - T_A) \quad (4)$$

where α is the thermal coefficient, and the subscripts c, 1 and 2 refer to composite wire, core and sheath, respectively. The residual stress of composite wire as a whole before loading, $\sigma_{c,0}$, should be zero. When the sheath behaves elastically, this condition is expressed as

$$\sigma_{c,0} = E_1 V_1 e_{r1} + E_2 V_2 e_{r2} = 0 \quad (5)$$

where V is the volume fraction. Combining Equations 3 to 5, we have

$$\alpha_c = (\alpha_1 E_1 V_1 + \alpha_2 E_2 V_2)/(E_1 V_1 + E_2 V_2) \quad (6)$$

When e_{r2} exceeds e_y, the sheath behaves plastically. In such a case, the condition that $\sigma_{c,0}$ should be zero is expressed as

$$\sigma_{c,0} = E_1 V_1 e_{r1} + V_2[(1 - \omega)\tau_y + \omega E_2 e_{r2}] = 0 \quad (7)$$

Combining Equations 3, 4 and 7, we have

$$\alpha_c = -(1 - \omega)\sigma_y V_2/[(T - T_A)(E_1 V_1 + \omega E_2 V_2)] + (\alpha_1 E_1 V_1 + \alpha_2 \omega E_2 V_2)/(E_1 V_1 + \omega E_2 V_2) \quad (8)$$

e_{r1} and e_{r2} can be calculated by substituting Equation 8 into Equations 3 and 4, respectively.

In the present calculation, following values were used: E_1 (room temperature) = 130 GPa [8], E_1 (77 K) = 130 GPa (assumed), E_2 (room temperature) = 71 GPa [9], E_2 (77 K) = 77 GPa, $\alpha_1 = 11.5 \times 10^{-6}\,K^{-1}$ [8], $\alpha_2 = 20.6 \times 10^{-6}\,K^{-1}$ [9], σ_y (room temperature) = 11.2 MPa (measured in this work), σ_y (77 K) = 13.2 MPa (measured), ω (room temperature) = 0.0080 (measured), ω (77 K) = 0.0091 (measured), T_A = 1193 K and T = 293 and 77 K. The values of α_1 and α_2 stated above were for the temperature range from room temperature to about 720 K [8, 9], but they were, to a first approximation, assumed to be the same in the temperature range in the present work.

Substituting the above values and the value of V measured for respective sample in this work, e_{r2} was calculated to be higher than e_y for all samples. This means that the sheath has yielded in tension before stressing. Therefore, when tensile stress, σ_c, is applied to a composite, the strain of the composite as a whole, e_c, is given by

$$e_c = \sigma_c/(E_1 V_1 + \omega E_2 V_2) \quad (9)$$

The exerted stress on the core, σ_1, at applied stress, σ_c, is given by

$$\sigma_1 = E_1(e_c + e_{r1}) \quad (10)$$

Combining Equations 3 and 8 to 10, we have

$$\sigma_{1u} = E_1\{[\sigma_c' - (1 - \omega)\sigma_y V_2 + (\alpha_2 - \alpha_1)(T - T_A)\omega E_2 V_2]/(E_1 V_1 + \omega E_2 V_2)\} \quad (11)$$

Substituting the aforementioned values of α, ω, σ_y, e, T and T_A, and measured values of V_1, and V_2 and σ_c' (stress of composite at fracture of the oxide) into Equation 11, we can estimate the cracking stress of the oxide, σ_{1u}.

In the R, S, RG, RGP and DP samples, once cracked, the oxide was cracked continually into shorter lengths with increasing applied stress. The stress of the composite at the second and following

crackings of the oxide increased in comparison with that at the first cracking, as shown in Fig. 3, because the first fracture is caused by the largest defect and the unfractured portion contains smaller defects than the largest one. The cracking stresses for the second and following crackings can roughly be estimated by substituting the composite stress at the respective drop in the stress–strain curves as σ_c' into Equation 11 within the range of a small number of crackings where the stress exerted on the oxide can be expressed by Equation 10.

3.2.2. Estimated values of cracking stress of the oxide

As stated above, because the number of cracks in the D sample could not be read from the stress–strain curve, the cracking stress was estimated from the stress at A in Fig. 3. Thus estimated values for D sample will be shown in parentheses.

The estimated values of the first and fifth cracking stress of the oxide at room temperature and 77 K are presented in Figs 7 and 8, respectively. The following features are seen from Figs 7 and 8.

1. The cracking stress of the present oxide was 50 MPa at most, being far lower than that of the superconducting Nb_3Sn compound (800 to 2000 MPa [10, 11]).
2. The larger the amount of working (swaging and rolling), the higher became the cracking stress.
3. The pressing treatment raised the cracking stress.
4. The cracking stress for drawn samples (D samples) was low in comparison with that in other samples.
5. The cracking stress for the fifth cracking was much higher than that of the first cracking, suggesting that the scatter in size of defects contained in the oxide was very large.
6. The cracking stress at room temperature was nearly the same as that at 77 K.

3.3. Critical current without externally applied stress

Fig. 9 shows the critical current density, J_{c0}, for 10 mm gauge length without externally applied stress. The following features may be seen from Fig. 9.

1. The higher the amount of working, the higher became the critical current density.

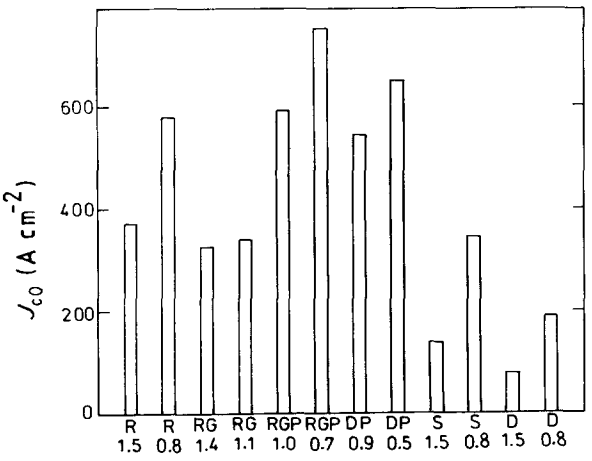

Figure 9 Critical current density, J_{c0}, of the oxide without externally applied stress for 10 mm length (average of three samples).

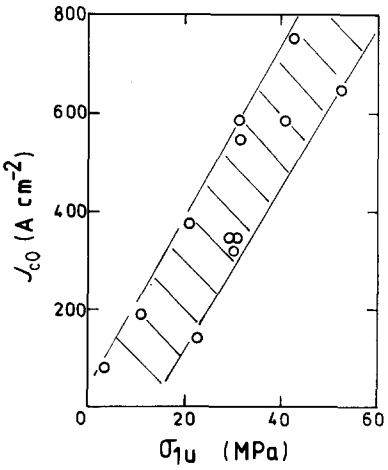

Figure 10 Correlation of critical current density, J_{c0}, to the cracking stress, σ_{1u}, of the oxide at first cracking at 77 K.

2. Pressing treatment was effective in raising the current density.
3. The current density of D samples was lower than that of other samples.

In the present samples, there was a strong correlation between critical current density, J_{c0}, and cracking stress of the oxide, σ_{1u}, as shown in Fig. 10 where the stress to cause first cracking at 77 K is taken as σ_{1u} for the stresses to cause first and fifth crackings at room temperature and 77 K, all of which showed the same correlation to the critical current density. In the present samples, the critical current is controlled by the weak links such as grain boundaries and defects. The cracking stress is also controlled by them. Thus, the controlling factors are, in a sense, common for critical current and cracking stress. From this point, the correlation between critical current and cracking stress shown in Fig. 10 could be explained to a first approximation. Of course, the controlling factors for the critical current are not completely the same as those for cracking stress. For instance, texture structure with the preferred (0 0 1) planes in rolled samples can increase J_{c0} [12]. Therefore, further investigation is needed to clarify the correlation between them. However, it should be emphasized that, for the present annealing condition (1193 K, 43.2 ksec), the preparation method to yield high cracking stress is favourable also for critical current density, at least empirically.

3.4. Change in critical current due to externally applied stress

In all samples, the critical current was reduced with increasing applied stress on the composite, σ_c. The change of critical current density as a function of σ_c for the R, S, RG, RGP and DP samples was approximately similar in all cases, but the change for these samples was quite different from that for the D sample. Fig. 11 shows the typical changes in critical current density, J_c, at 77 K at 0 T with increasing applied stress for the former (R1.5) and the latter (D0.8) samples, respectively. The following relations between fracture behaviour and critical current density can be mentioned.

1. The variation of J_c for the gauge length of 10 mm as a function of applied stress, σ_c, for samples except

the D sample, was approximately similar in that the reduction in J_c occurred rapidly beyond the critical stress, while the reduction in J_c of the D samples occurred rather gradually. This could be attributed to the difference in fracture behaviour. In the former samples, the cracking occurred suddenly at the cracking stress and fracture of the oxide occurred nearly perpendicular to the tensile axis, and the resultant crack size was large. The superconducting current path was entirely cut rapidly when the crack propagated entirely in a cross-section of the oxide, as shown in Fig. 4. Even when the propagation of the crack was suppressed, for instance by the pre-existing longitudinal crack, as shown in Fig. 5, the current path was cut in a high percentage of cases in the cracked cross-section. Thus the critical current density dropped suddenly upon cracking in the former samples. On the other hand, in the D sample, at low applied stress, the cracks did not propagate at once. They propagated gradually. This fracture behaviour of the oxide could leave the current path. With further increasing applied stress, as the number and size of micro-cracking increased gradually, the current path decreased gradually and finally diminished.

In this work, the critical current density became very low at high applied stress, but it did not fall to zero. This result is, however, unreasonable. The reason for this result may be attributed to the employment of the criterion of $1\ \mu V\ cm^{-1}$ for determination of critical current and the low resistance of silver. Under this condition, the critical current values are not accurate when the current is very low.

2. There were big differences in the variation of J_c among the portions, especially in the former samples. In the example shown in Fig. 11, the portion 4–5 in the R1.5 sample showed a reduction at low applied stress but not portion 3–4. As the cracking stress of the oxide had a wide scatter, there were strong and weak portions. The strong portion could maintain the critical current up to high applied stress. As the fracture of the oxide occurred at first at the weakest portion, the reduction in critical current occurred in this portion. Once the weakest portion had fractured, the critical current of the sample as a whole became nearly zero because the current capacity of the sample was determined by the portion with the lowest capacity. With increasing applied stress, the second and then the third weakest portions fractured, and finally all portions fractured, resulting in a loss of current capacity in all portions. In this way, the loss in current capacity was strongly dependent on the cracking stress and its scatter of oxide.

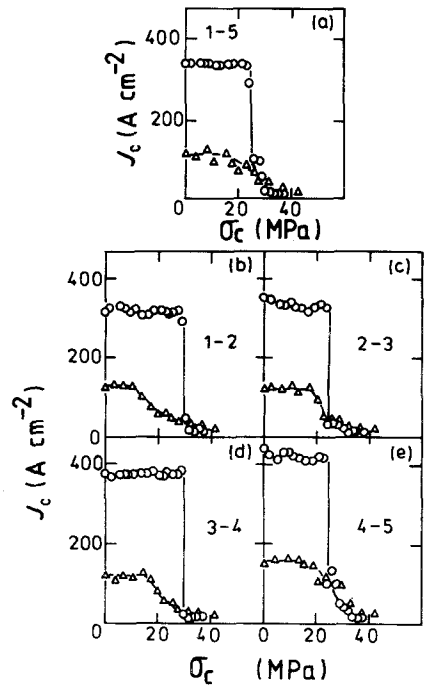

Figure 11 Changes in J_c of the (○) R1.5 and (△) D0.8 samples with increasing σ_c for (a) the whole length (10 mm) corresponding to 1–5 in Fig. 1, and (b to e) that for divided length 2.5 mm corresponding to $i - i + 1$ (i = 1 to 4) in Fig. 1.

4. Conclusions

Silver-sheathed $Ba_2YCu_3O_{7-x}$ superconducting composite wires were fabricated by swaging, rolling, drawing and pressing methods, and the cracking stress of the oxide at room temperature and 77 K, and the critical current density at 0 T at 77 K of the $Ba_2YCu_3O_{7-x}$ oxide were measured. The main results can be summarized as follows.

1. The stress–strain curves of the composite wires fabricated by swaging, rolling and pressing methods showed many drops in stress. Each drop corresponded to fracture of the oxide. At high applied stress, the oxide showed multiple fracture.

2. The stress–strain curves of the composite wires fabricated by the drawing method showed no apparent drops in stress. Many micro-cracks were observed in these wires. In these wires, the cracks did not necessarily propagate at once at low applied stress, but they grew gradually with increasing applied stress.

3. The critical current density before stressing was dependent on the fabrication method: the pressing method yielded high density but not the drawing method. It was also dependent on the amount of working: the higher the amount of working, the higher became the density.

4. There was a correlation between critical current density and cracking stress: the higher the cracking stress, the higher became the critical current density.

5. The critical current density was reduced with increasing applied stress, due to cracking of the oxide.

6. The reduction in critical current with increasing applied stress was dependent on the fabrication method: the swaging, rolling and pressing methods resulted in relatively high endurance against stress in comparison with the drawing method.

7. The reduction in critical current with increasing applied stress was dependent on the portion: it occurred at high applied stress when the cracking stress of the oxide in the measured portion was high.

8. The strength of the oxide in the present samples was very low in comparison with that of superconducting Nb_3Sn compound.

9. Among the present fabrication methods, the rolling swaging and pressing methods gave higher strength than the drawing method. There was a tendency that the higher the amount of working, the higher

the strength as well as the critical current density became.

10. The strength of the oxide had a strong dependence on length: the longer the length, the lower the strength became.

11. The strength at room temperature was little different from that at 77 K.

Acknowledgements

The authors thank Messrs I. Nakagawa and T. Unesaki for their help in SEM studies, and The Ministry of Education, Science and Culture of Japan for the grant-in-aid (no. 63055026).

References

1. M. K. WU, J. R. ASHBURN, C. J. TORNG, P. H. HOR, R. L. MENG, L. GAO, Z. J. HUANG, Y. Q. WANG and C. W. CHU, *Phys. Rev. Lett.* **58** (1987) 908.
2. I. PFEIFFER and E. SPRINGER, *Z. Metallkde.* **68** (1977) 667.
3. S. OCHIAI, K. OSAMURA and T. UEHARA, *J. Mater. Sci.* **21** (1986) 1027.
4. S. OCHIAI and K. OSAMURA, *ibid.* **22** (1987) 2175.
5. *Idem, Acta Metall* **36** (1988) 1607.
6. A. KELLY and W. R. TYSON, *J. Mech. Phys. Solids* **13** (1965) 329.
7. S. OCHIAI and K. OSAMURA, *Z. Metallkde.* **77** (1986) 255.
8. N. M. ALFORD, J. D. BIRCHALL, W. J. CLEGG, M. A. HARMER, K. KENDALL and D. H. JONES, *J. Mater. Sci.* **23** (1988) 761.
9. C. D. COXE, A. S. MCDONALD and G. H. SISTARE, in "Metals Handbook", 9th Edn (American Society for Metals, Ohio, 1979) p. 671.
10. S. OCHIAI, T. UEHARA and K. OSAMURA, *J. Mater. Sci.* **21** (1986) 1020.
11. S. OCHIAI, K. OSAMURA and T. UEHARA, *ibid.* **22** (1987) 2163.
12. T. TAKAYAMA, Master thesis, Kyoto University (1989).

Received 6 April
and accepted 28 September 1989